Sensitivity of remote sensing–derived phytoplankton productivity to mixed layer depth: Lessons from the carbon-based productivity model

Svetlana Milutinović,[1,2,3] Michael J. Behrenfeld,[4] Johnny A. Johannessen,[1,3] and Truls Johannessen[3,5]

[1]   Mixed layer depth (MLD) has long been recognized as having an important influence on underwater light budget and, thus, net primary productivity (NPP) of phytoplankton. The depth- and wavelength-integrated carbon-based productivity model (DWI CbPM) is one of a few productivity algorithms that explicitly use information on MLD to estimate ocean NPP from remote sensing observations. This study evaluates the sensitivity of NPP estimates from the DWI CbPM to MLD input by using MLD fields from four different ocean models. Owing to the effect of MLD on light availability, the model NPP is generally inversely related to MLD, but the strength of this relationship is highly variable. In most of the ocean, it exhibits a seasonal character. In summer, NPP at middle and high latitudes can show substantial sensitivity to subtle changes in MLD, but is largely robust to strong MLD variability in winter. An opposite seasonal pattern is encountered in subtropical ocean gyres. A lack of seasonality is observed in tropical areas, among which only the equatorial Pacific displays strong response of NPP to small or moderate changes in MLD. We find that the spatial and temporal variability of the MLD-NPP relationship can be explained by nonlinearity and light saturation/limitation thresholds indicated in the DWI CbPM, as well as the influence of surface irradiance (I_0) and diffuse attenuation coefficient for downwelling light at 490 nm ($K_d(490)$). NPP is sensitive to varying MLD only if coincidental I_0 and $K_d(490)$ values are such that combined with the coexisting differences in MLD estimates, they have potential to give effective differences in light saturation/limitation of photosynthesis.

Citation: Milutinović, S., M. J. Behrenfeld, J. A. Johannessen, and T. Johannessen (2009), Sensitivity of remote sensing–derived phytoplankton productivity to mixed layer depth: Lessons from the carbon-based productivity model, *Global Biogeochem. Cycles*, *23*, GB4005, doi:10.1029/2008GB003431.

1.   Introduction

[2]   The dominant primary producers in the ocean are phytoplankton, microscopic photosynthetic organisms suspended in the illuminated part of water column. They are responsible for roughly half of the global annual photosynthetic net primary productivity (NPP), which is the amount of fixed carbon available for the first heterotrophic level in an ecosystem [*Field et al.*, 1998]. Environmental forcing controls spatiotemporal changes in phytoplankton abundance and community composition by affecting the key determinants of marine photosynthesis: mixed-layer light availability, concentration of macronutrients and micronutrients, and the ambient temperature [*Behrenfeld et al.*, 2002a; *Field et al.*, 1998]. Owing to a tight coupling between photosynthesizers and higher trophic levels via transfer of matter and energy, any environmental changes imposed on phytoplankton are bound to resonate across food webs, thereby potentially affecting functioning and structure of marine ecosystems [*Cloern and Dufford*, 2005; *Duffy and Stachowicz*, 2006; *Riebesell et al.*, 2007]. Phytoplankton are also likely to impose feedbacks on the future climate system [*Falkowski et al.*, 1998; *Frouin and Iacobellis*, 2002; *Gabric et al.*, 2004]. Physical-chemical-biological interactions often involve a high degree of complexity and nonlinearity [*Jickells et al.*, 2005], making them complicated to understand. The present lack of understanding restricts our ability to predict future consequences of ongoing man-made climate perturbations. Clarifying controls on primary productivity and related responses and feedbacks has been identified as a key goal of global change research [*Falkowski et al.*, 2000; *Geider et al.*, 2001].

[1]Nansen Environmental and Remote Sensing Center, Bergen, Norway.
[2]Bjerknes Centre for Climate Research, Bergen, Norway.
[3]Geophysical Institute, University of Bergen, Bergen, Norway.
[4]Department of Botany and Plant Pathology, Oregon State University, Corvallis, Oregon, USA.
[5]Also at Bjerknes Centre for Climate Research, Bergen, Norway.

[3] An essential requirement for achieving this goal is measurements of NPP and quantification of its variability in space and time. However, ship-based NPP measurements are insufficient [*Carr et al.*, 2006] and need to be complemented with satellite observations [*Behrenfeld et al.*, 2002a]. Satellite ocean color sensors have been routinely producing a global optical view of the ocean surface. The sensors measure spectral characteristics of water-leaving radiance, which are influenced by the type and concentration of optically active materials in seawater, such as chlorophyll and suspended particles [*International Ocean Colour Coordinating Group (IOCCG)*, 2000]. It is thus possible, by deploying inversion models of optical properties, to quantify these materials from remotely sensed optical signal [*Garver and Siegel*, 1997]. Most NPP models use chlorophyll as an index of phytoplankton biomass, because it is easily obtainable from remote sensing and is the only pigment found in all phytoplankton taxa [*Geider and MacIntyre*, 2002]. However, there are two main issues associated with this chlorophyll-based approach. First, variations in chlorophyll are not exclusively a result of variations in biomass, but can also be caused by physiological adjustment of intracellular pigment concentrations to non-optimal light, nutrient, and temperature levels [*Behrenfeld et al.*, 2005]. Second, the direct conversion of chlorophyll concentration to NPP requires an empirically established scaling parameter, which should account for variability in carbon assimilation efficiency. This parameter cannot be assessed with sufficient accuracy [*Behrenfeld and Falkowski*, 1997a] and is considered responsible for the poor performance of chlorophyll-based algorithms [*Behrenfeld and Falkowski*, 1997b; *Behrenfeld et al.*, 2002b; *Campbell et al.*, 2002].

[4] Recently, *Behrenfeld et al.* [2005] developed an alternative, carbon-based, approach to NPP calculations. This was made possible by the advent of semianalytical ocean color models, which are able to simultaneously quantify both chlorophyll and backscattering by particles [*Garver and Siegel*, 1997; *Maritorena et al.*, 2002; *Siegel et al.*, 2002]. The carbon-based productivity model (CbPM) of *Behrenfeld et al.* [2005] bypasses the main weaknesses of chlorophyll-based algorithms by deriving information on phytoplankton physiology directly from remote sensing products. The CbPM calculates phytoplankton biomass from particulate backscattering coefficient, which shows an empirical correlation with particulate organic carbon in case 1 waters, i.e., open ocean [*Loisel et al.*, 2001; *Stramski et al.*, 1999]. Physiological information is then extracted from variability in chlorophyll:carbon (Chl:C) ratios on the basis of the extensive laboratory-derived knowledge on ecophysiology.

[5] Physiological responses to varying growth irradiance (I_g) are an important factor influencing both phytoplankton Chl:C ratios and photosynthetic assimilation efficiencies. Mixed layer depth (MLD) is a crucial regulator of I_g, as well as nutrient availability [*Mann and Lazier*, 1996]. While accurate MLD estimates are vitally important for NPP estimates [*Westberry et al.*, 2008], few studies have examined the sensitivity of NPP models to MLD perturbations. *Carr et al.* [2006] analyzed sensitivity of six NPP models to widely varying MLD at 11 representative locations in all ocean basins and reported up to a factor of 2 impact. *Friedrichs et*

al. [2009] investigated the effect of uncertainties in MLD input (±20 m) on productivity estimates in the tropical Pacific for seven NPP models. They found that MLD uncertainties severely limit the skills of most of the studied models. Among them, both depth- and wavelength-integrated (DWI) [*Behrenfeld et al.*, 2005] and depth- and wavelength-resolved (DWR) [*Westberry et al.*, 2008] versions of the CbPM were considered. Interestingly, the DWR CbPM was largely robust to MLD perturbations in the region of interest, while the DWI CbPM was the most sensitive among the inspected models.

[6] Motivated by those findings, here we address more extensively and in more detail the sensitivity of the DWI CbPM to changes in input MLD. While our study focuses on a particular NPP model, its results may also contribute to better understanding of similar NPP models that use MLD to describe phytoplankton physiological acclimation to changing light conditions (i.e., photoacclimation). Furthermore, the importance of mixing depth variability is intrinsic to all NPP estimates, regardless of whether photoacclimation is included in a given model formulation. In other words, NPP models that do not include light dependence in their formulation of assimilation efficiencies are subject to large errors associated with the full range of photoacclimation, whereas those models that do include a photoacclimation term are subject to smaller errors associated with uncertainties in assessing I_g.

[7] Sensitivity of the DWI CbPM−derived NPP estimates is examined using MLD fields produced by four different ocean models. Results of the sensitivity experiments are analyzed both globally and in two oceanographically and ecologically distinct North Atlantic provinces: the subpolar and subtropical gyres.

2. Methods

2.1. Productivity Algorithm

[8] The DWI version of the CbPM is presented by the following expression [*Behrenfeld et al.*, 2005]:

$$NPP = C_{sat} \times \left[2 \text{ cell divisions d}^{-1} \times \frac{Chl : C_{sat}}{0.022 + (0.045 - 0.022)e^{-3I_g}} \right.$$
$$\left. \times \left(1 - e^{-3I_g}\right) \right] \times \frac{-\ln(0.01)}{K_d(490)} \times \frac{0.66125 I_0}{I_0 + 4.1}, \quad (1)$$

where the terms C_{sat} and I_g are defined as

$$C_{sat} = \left(b_{bp}(443) - 0.00035 \text{ m}^{-1}\right) \times 13{,}000 \text{ mg C m}^{-2}, \quad (2)$$

$$I_g = I_0 \times e^{-K_d(490) \times MLD/2}. \quad (3)$$

Vertically integrated net primary productivity (NPP [mg C m^{-2} d^{-1}]) is calculated as a product of satellite-derived surface phytoplankton carbon biomass (C_{sat} [mg C m^{-3}]) and growth rate, scaled to the depth of the euphotic zone, while taking into account changes in photosynthetic rate with depth. C_{sat} (see equation (2)) is determined from particulate backscattering coefficient at 443 nm ($b_{bp}(443)$ [m^{-1}]), which

Table 1. Overview of the Main Features of Mixed Layer Depth Data Sets Used in This Study

Model Acronym	Spatial Coverage	Temporal Coverage	Horizontal Resolution	Vertical Coordinates	Basis of MLD Definition	Vertical Mixing Scheme
TOPS	global	October 1997 to September 2004	$1° \times 1°$	fixed depth	temperature	level 2 turbulence closure theory of *Mellor and Yamada* [1974]
MICOM1	global	October 1997 to September 2004	location-dependent ($\sim$40 to $\sim$200 km)	isopycnic	heat, salinity, and momentum fluxes	kinetic energy (KE) parameterization of *Gaspar et al.* [1990]
MICOM2	North Atlantic	October 1997 to September 2003	location-dependent ($\sim$20 to $\sim$40 km)	isopycnic	heat, salinity, and momentum fluxes	kinetic energy (KE) parameterization of *Gaspar et al.* [1990]
HYCOM	North Atlantic	October 1997 to September 2004	location-dependent ($\sim$11 to $\sim$16 km)	hybrid (fixed depth in the mixed layer)	density	*K* profile parameterization (KPP) of *Large et al.* [1994]

is first corrected for a stable background contribution from nonalgal particles (0.00035 m^{-1}), and then multiplied by a scaling factor ($13,000$ mg C m^{-2}) that relates $b_{bp}(443)$ to algal biomass. Phytoplankton growth rate (expressed in cell divisions per day) is computed from a maximum growth rate estimate based on observations in natural communities (2 cell divisions d^{-1}) [*Banse*, 1991], then adjusted to account for decreases in growth caused by suboptimal nutrient, temperature, and light conditions. The third term in equation (1) embodies reductions in growth rate due to combined effects of nutrient and temperature limitation, using the ratio between surface chlorophyll (Chl [mg Chl m^{-3}]) and C_{sat} (Chl: C_{sat}, given in the numerator) relative to the maximum possible Chl:C ratio at a given irradiance (in the denominator). The fourth term determines the degree of light limitation from growth irradiance (I_g [mol photons m^{-2} h^{-1}]), which is taken to be the median light intensity for phytoplankton in the mixed layer. I_g (see equation (3)) is a function of photosynthetically available radiation at the sea surface (I_0 [mol photons m^{-2} h^{-1}]), the diffuse attenuation coefficient for downward irradiance at 490 nm ($K_d(490)$ [m^{-1}]), and mixed layer depth (MLD [m]). The DWI CbPM uses MLD explicitly to determine average exposure of phytoplankton to light, while the indirect influence of MLD on nutrient availability is captured by Chl:C_{sat} variability for a given I_g. $K_d(490)$ is also used to calculate the euphotic depth, defined here as the depth at which irradiance is reduced to 1% of its sea surface value (the fifth term in equation (1)). Finally, the sixth term in equation (1) accounts for the loss in potential NPP due to light limitation.

2.2. Satellite Data

[9] Remote sensing input variables for the DWI CbPM were level 3 composites based on the fifth reprocessing of satellite ocean color observations taken by the Sea-viewing Wide Field-of-view Sensor (SeaWiFS). These data sets consist of global monthly mean values, presented on an equal area grid with the bin size of approximately 9 km × 9 km. The grid characteristics are discussed in detail by *IOCCG* [2004]. I_0 and $K_d(490)$ are standard SeaWiFS products distributed by the Ocean Color Web at ftp://oceans.gsfc.nasa. gov/SeaWiFS/Binned/Monthly/. Chl and $b_{bp}(443)$ were computed by the Garver-Siegel-Maritorena model version 1 (GSM01) [*Garver and Siegel*, 1997; *Maritorena et al.*, 2002; *Siegel et al.*, 2002]. GSM01 Chl exhibits similar agreement with coincidental in situ measurements of chloro-

phyll as the standard SeaWiFS chlorophyll product [*Siegel et al.*, 2005]. Too few reliable in situ observations of $b_{bp}(443)$ in the open ocean are available to enable estimates of the uncertainty in GSM01 $b_{bp}(443)$ retrievals (S. Maritorena, personal communication, 2006).

2.3. Model-Based MLD Fields

[10] Although MLD climatologies could be used in the DWI CbPM, it is more advisable to use MLD generated by ocean models, in order to capture information on interannual variability [*Behrenfeld et al.*, 2005]. MLD data sets generated by four different ocean models were used in the sensitivity experiments. Key model characteristics and methods for calculation of MLD are summarized in Table 1. Daily model MLD values were averaged to produce monthly mean fields collocated with the satellite products. Since all MLD data sets had coarser horizontal resolution than the remote sensing data sets, the nearest-neighbor interpolation scheme was used to place them on the SeaWiFS 9-km grid prior to the experiments.

[11] The first MLD data set was produced by the Thermodynamic Ocean Prediction System (TOPS), a model of the Fleet Numerical Meteorology and Oceanography Center (FNMOC), Monterey, California [*Clancy and Martin*, 1981; *Clancy and Pollak*, 1983; *Clancy and Sadler*, 1992]. This data set was used in the original DWI CbPM calculations by *Behrenfeld et al.* [2005]. TOPS provides global coverage on $1° \times 1°$ horizontal grid, while the vertical axis extends down to 400 m, with coordinates constrained to fixed depths. The upper boundary conditions (i.e., surface wind stress and heat fluxes) are provided by the Navy Operational Global Atmospheric Prediction System (NOGAPS). The Level 2 turbulence closure theory of *Mellor and Yamada* [1974] is used to represent the effects of vertical mixing. MLD is the depth at which the temperature drops by $0.5°C$ from the value at the sea surface.

[12] The second MLD data set is an output of a global version of the Miami Isopycnic Coordinate Ocean Model (MICOM) [*Bleck and Smith*, 1990; *Bleck et al.*, 1992], run at the Nansen Environmental and Remote Sensing Center (NERSC), Bergen, Norway. This data set is supplied on an irregular grid, with two poles placed over North America and Eurasia, respectively. Such grid design provides enhanced spatial resolution ($\sim$40 km) in the Nordic Seas, while grid cells in the Southern Ocean are $\sim$200 km. This MLD data set is referred to here as the MICOM1 MLD data set. MICOM

represents the ocean water column with 26 isopycnal layers. While the 25 interior layers have prescribed densities, the uppermost layer is the thermodynamically active mixed layer. Its density is vertically uniform, but varies horizontally and in time. MICOM does not allow the mixed layer to get shallower than ~20 m. MICOM is forced by daily mean fluxes of fresh water, heat and momentum from the NCEP/NCAR Reanalysis Project at the National Oceanic and Atmospheric Administration (NOAA). MLD is determined as a prognostic variable, based on the available turbulent energy, by means of a simple eddy kinetic energy model from *Gaspar et al.* [1990].

[13] The third MLD data set, covering only the North Atlantic, is a product of a North Atlantic version of MICOM from NERSC [*Hátún et al.*, 2005]. This data set is generated in a similar manner as MICOM1 but has an improved spatial resolution in the North Atlantic (from ~20 km in the Nordic Seas to ~40 km in the subtropical gyre). This third MLD model is referred to here as MICOM2.

[14] The fourth MLD data set, also limited to the North Atlantic, is generated by NERSC's version of the Hybrid Coordinate Ocean Model (HYCOM) [*Bleck*, 2002]. In the mixed layer, this particular version of HYCOM employs constant depth vertical coordinates. Owing to a curvilinear grid used by HYCOM, horizontal resolution of this data set varies from ~11 km to ~16 km, depending on the ocean region. HYCOM uses forcing fields in the form of wind stress, heat, and freshwater fluxes from the European Centre for Medium Range Weather Forecasts (ECMWF). Upper ocean mixing processes are parameterized using the vertical mixing scheme of *Large et al.* [1994]. MLD is calculated as the depth at which the density of seawater increases by 0.125 g cm^{-3} compared to the surface value.

[15] Scarcity of hydrographic measurements precludes us from making any definitive evaluation of the accuracy of MLD estimates from the four models. While today measurements from Argo floats have reached a very good spatial coverage, it was not the case during the time period of this study (1997–2004).

2.4. Sensitivity Experiments

[16] MLD fields from the four models described above exhibit significant differences because they are generated on different horizontal and vertical grids, using different environmental forcing, mixing parameterizations and definitions of MLD. This range of variability in MLD assessments serves the purpose of our sensitivity experiments.

[17] To examine the influence of MLD variability on NPP, four sensitivity experiments were performed. Each DWI CbPM run was executed using the same data sets of SeaWiFS-derived monthly mean $b_{bp}(443)$, Chl, $K_d(490)$ and I_0. The runs differed only in the choice of MLD data set.

[18] The DWI CbPM expression for phytoplankton carbon biomass (equation (2)) is likely to fail in optically complex waters, where suspended inorganic particles load is not functionally related to phytoplankton [*Behrenfeld et al.*, 2005]. Thus, exclusion of shelf regions (here defined as shallower than 200 m) from the analysis was used as a simple way to delineate those waters. In addition, the Arctic waters (i.e., latitudes higher than 75°N) were disregarded owing to poor satellite coverage and persistent sea ice. No correction for missing satellite data was employed.

[19] In section 3, we first present results of sensitivity experiments with the two global MLD data sets (TOPS and MICOM1) over the entire world ocean. Subsequently, results based on all four MLD data sets are presented for the North Atlantic subpolar gyre and the eastern part of the North Atlantic subtropical gyre.

3. Results

3.1. Global Ocean

[20] To facilitate the analysis of the results, twelve respective monthly mean MLD and NPP fields were produced by averaging over the 7-year period from October 1997 to September 2004. The boreal winter/austral summer is presented by average January values (Figures 1a, 1b, 1g, and 1h). July averages represent the boreal summer/austral winter (Figures 1d, 1e, 1j, and 1k). On further mention of seasons, both hemispheres are implied (e.g., "summer" means both boreal and austral summer), unless specified otherwise. The mixed layer from either model is considerably deeper in winter in each hemisphere, particularly at high and middle latitudes, where NPP is extremely low. On the other hand, these latitudes become very productive in summer, which coincides with shoaling of the mixed layer. In contrast, lower latitudes show more moderate seasonal variability in MLD and NPP. Whereas equatorial waters are highly productive throughout the year, subtropical regions exhibit sustained low NPP.

[21] To compare results from the different MLD and NPP estimates, difference values (hereafter denoted by Δ) for each average month were calculated by subtracting MICOM1 MLD and NPP mean from the equivalent TOPS mean. In general, comparison of ΔMLD (Figures 1c and 1f) with corresponding ΔNPP (Figures 1i and 1l) reveals an inverse relationship between MLD and NPP. As indicated in equations (1) and (3), an increase in MLD can only cause a decrease in estimated I_g, and hence in NPP. However, there are instances in which even a very strong ΔMLD makes little difference for NPP estimates. For example, the pronounced wintertime ΔMLD in the North Atlantic Current (Figure 1c) bears little effect on NPP (Figure 1i). Also, there are regions having clearly distinguishable ΔMLD values, but similar ΔNPP values. Such a case can be easily identified in average January in the middle- to high-latitude South Atlantic (Figures 1c and 1i), where there are two distinct areas with comparable ΔNPP ($\sim-700 \text{ mg C m}^{-2} \text{ d}^{-1}$), yet differing in terms of ΔMLD values by an order of magnitude (~30 m in the equatorward area versus ~300 m in the poleward area). Moreover, it is possible that a slight variability in MLD gives rise to a large variability in NPP, as for example in the middle- to high-latitude North Atlantic in summer (Figures 1f and 1l). All such cases can be explained by the nonlinearity of the relationship between I_g and MLD, as well as the influence of I_0 and $K_d(490)$ on it (equation (3)), and the existence of light saturation and limitation thresholds (indicated in the fourth term of equation (1)). A detailed discussion of these effects will follow in section 4.
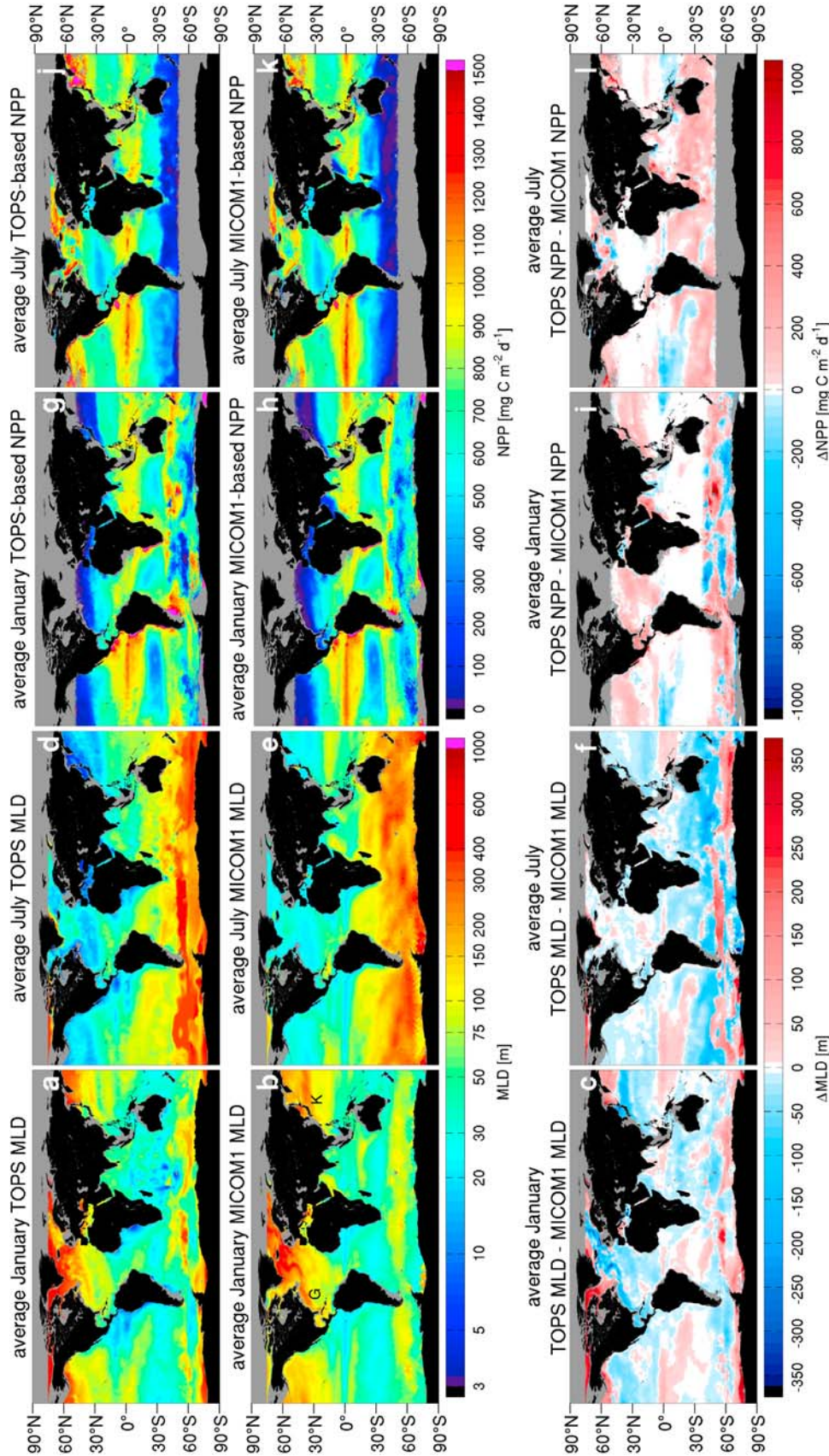
Figure 1. Temporal averages for the months of January and July between 1998 and 2004 of the mixed layer depth values modeled by TOPS and MICOM1 (MLD [m]), the associated net primary productivity estimates from the DWI CbPM (NPP [mg C m^{-2} d^{-1}]) and the corresponding differences in MLD (ΔMLD [m]) and NPP (ΔNPP [mg C m^{-2} d^{-1}], respectively. The differences are calculated by subtracting a given MICOM1 estimate from the equivalent TOPS estimate (Figure 1c = Figure 1a – Figure 1b; Figure 1d – Figure 1e; Figure 1f = Figure 1d – Figure 1e; Figure 1i = Figure 1g – Figure 1h; Figure 1l = Figure 1j – Figure 1k). Thus, negative ΔMLD means that TOPS MLD is shallower than MICOM1 MLD, while positive ΔMLD means the opposite. Grey color indicates shelf (<200 m), the Arctic (>75°N), and pixels with no MLD data or ocean color observations (e.g., due to cloud cover, polar darkness, or sea ice). Letters G and K in Figure 1b denote the Gulf Stream and the Kuroshio Current, respectively.
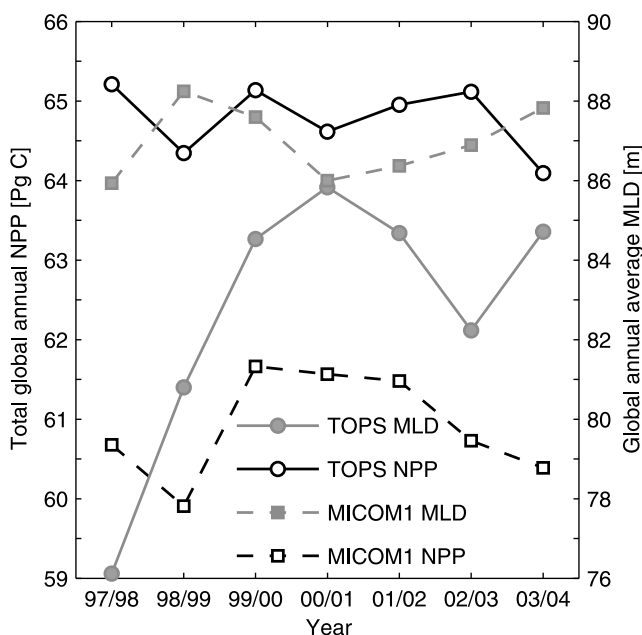
Figure 2. Global annual mean MLD [m] from TOPS and MICOM1, with corresponding total global annual NPP calculated by the DWI CbPM, presented in petagrams (10^{15} grams) of carbon [Pg C]. The MLD values were calculated as global averages over seven consecutive 12-month periods ranging from October to September between 1997 and 2004 (e.g., year 1997/1998 is the period October 1997 to September 1998). The NPP values were computed by summing up global monthly NPP over the same 12-month periods. Note that the y axes do not start from zero. No interpolation for cloudy bins has been performed, and MLD values in those bins have been disregarded. Thus, these global values should not be regarded as complete, and any conclusions about interannual trends should be made with caution. However, cloudiness does not present a problem when values from the same time step are compared. Data from shelf regions (<200 m) and the Arctic (>75°N) have been omitted.

[22] Figures 1c and 1f show that the prominent ΔMLD values are frequent in winter, especially at high latitudes, where the mixed layer is particularly deep. The absolute values of ΔMLD (|ΔMLD|) in the sub-Arctic regions and the Southern Ocean sometimes reach more than 300 m. However, the observed effect of large |ΔMLD| at high to middle latitudes is modest, as |ΔNPP| spans from zero to maximally a few hundred mg C m^{-2} d^{-1} (Figures 1i and 1l). For example, at a location along the North Atlantic Current track, average January ΔMLD of ~−360 m leads to a ΔNPP ranging between ~40 and ~70 mg C m^{-2} d^{-1}.

[23] In summer, a shallow mixed layer is fully developed and MLD variability at middle to high latitudes becomes more restrained, particularly in the northern hemisphere, where |ΔMLD| is often on the order of only a few meters (Figure 1f). However, at these latitudes NPP is much more responsive to the summer ΔMLD (Figure 1l). For instance, at some locations in the North Pacific, average July ΔNPP

reaches more than 1000 mg C m^{-2} d^{-1}, which corresponds to ΔMLD of merely ~−15 m. Similarly, in the Southern Atlantic, average January ΔMLD of ~45 m leads to ΔNPP of nearly −1000 mg C m^{-2} d^{-1}.

[24] In contrast to middle and high latitudes, subtropical gyres are characterized by moderate winter |ΔMLD| (Figures 1c and 1f). Only along the Gulf Stream and the Kuroshio Current does |ΔMLD| reach above 100 m. Elsewhere in the subtropical gyres, |ΔMLD| rarely surpasses 50 m and often takes up values of ~25 m or less. Even so, winter |ΔNPP| values in the subtropics are generally similar to the largest |ΔNPP| values at higher latitudes (i.e., up to ~300 mg C m^{-2} d^{-1}; Figures 1i and 1l). In comparison, summer |ΔMLD| in the subtropical gyres is very subtle and rarely goes beyond 10 m. Its influence on ΔNPP is negligible, which contrasts with the effect observed during summer at higher latitudes.

[25] Contrary to the above mentioned regions, tropical areas show little seasonality in ΔMLD (Figures 1c and 1f) and ΔNPP (Figures 1i and 1l). In the equatorial zone of the Atlantic and Indian Oceans, |ΔMLD| is most often significantly below ~30 m, while |ΔNPP| is usually close to zero. Central equatorial Pacific, on the other hand, features larger |ΔMLD| (up to ~60 m), concurrent with |ΔNPP| of ~300 to ~400 mg C m^{-2} d^{-1}. This result agrees with the pronounced sensitivity of the DWI CbPM to MLD perturbations (±20 m) in the tropical Pacific, found by *Friedrichs et al.* [2009]. They reported the removal of MLD uncertainties might reduce the total root mean square difference for the DWI CbPM by as much as 40% and hence greatly improve the skill of the model in this region.

[26] Overall, findings reveal a clear pattern. In winter, |ΔMLD| increases substantially from the subtropics poleward, while an opposite and much weaker meridional gradient is found for |ΔNPP|. In summer, smaller |ΔMLD| is observed at all latitudes, with no distinct meridional gradient. However, summer ΔNPP in the subtropics is negligible, while it attains considerable values at middle and high latitudes. In comparison, equatorial regions display little seasonal variability in either ΔNPP or ΔMLD.

[27] Figure 2 presents global annual average MLD values from TOPS and MICOM1 along with related globally integrated annual NPP estimates. The TOPS MLD averages are consistently shallower and thus associated with higher NPP estimates. However, the interannual progression of global MLD values from either model is not perfectly mirrored in the direction of corresponding NPP, although the inverse relationship is largely obvious. This is, nevertheless, not unexpected, bearing in mind the nonlinearity involved in the DWI CbPM (equations (1) and (3)). The annual NPP values based on MICOM1 MLD are 5−7% lower than those based on TOPS MLD. This is not incompatible with the results of the sensitivity analysis performed by *Carr et al.* [2006] on six NPP models. They systematically varied MLD over a wide but realistic range of values at 11 geographically representative points in the world ocean. Some NPP models were largely insensitive to changes in MLD, but most showed up to a factor of 2 response, which is comparable with small-scale variability in NPP we discovered. However, the relative differences in global annual NPP estimates (Figure 2) are

Table 2. Descriptive Statistics of Respective MLD Values From TOPS, MICOM1, MICOM2, and HYCOM, and Their Associated NPP Values in North Atlantic Subpolar Gyre in Average March and July of the Period 1998–2003[a]

	MLD				NPP			
	TOPS	MICOM1	MICOM2	HYCOM	TOPS	MICOM1	MICOM2	HYCOM
	Average March							
Mean	294.1	380.3	366.8	652.5	14.3	12.7	18.3	6.2
Median	321.6	341.6	290.0	500.1	2.6	1.5	3.2	0.1
Minimum	47.5	47.4	23.4	40.8	0.0	0.0	0.0	0.0
Maximum	400.0	1305.4	1817.9	3206.3	1422.9	2908.4	1202.1	1119.7
2nd percentile	88.7	109.0	115.3	106.0	0.1	0.0	0.0	0.0
98th percentile	398.5	882.6	965.2	2177.5	119.3	104.4	129.3	63.9
	Average July							
Mean	32.0	30.3	29.5	20.1	867.8	836.3	845.1	1048.1
Median	28.1	29.5	28.8	20.7	871.7	836.1	838.2	1034.7
Minimum	3.8	20.3	20.2	2.9	0.0	46.1	149.1	359.6
Maximum	263.3	95.5	71.1	35.0	6017.3	6062.8	7088.0	8536.4
2nd percentile	9.9	21.9	21.1	10.4	70.6	443.7	523.4	678.1
98th percentile	105.3	46.8	42.3	25.3	1422.7	1208.9	1232.2	1486.8

[a]MLD, Mixed layer depth (values expressed in m); NPP, Net primary productivity (values expressed in mg C m^{-2} d^{-1}); TOPS, Thermodynamic Ocean Prediction System; MICOM, Miami Isopycnic Coordinate Ocean Model; HYCOM, Hybrid Coordinate Ocean Model. Shelf regions (<200 m) are not taken into account.

generally considerably smaller, because local short-term positive and negative differences are to a large extent canceled out in the process of temporal and spatial integration. Over the period October 1997 to September 2004, the TOPS-based annual NPP averages to slightly more than 64.5 Pg C, which is about 2.5 Pg C less than *Behrenfeld et al.* [2005] reported for the period 1997–2002. This difference is caused by not applying interpolation in cloudy regions in this study, while different time period, exclusion of certain parts of the global ocean and version of SeaWiFS data used for the DWI CbPM are likely of secondary importance.

[28] In the following text, regional characteristics of the relationship between MLD and NPP are examined in more detail by focusing on the North Atlantic subpolar and subtropical gyres.

3.2. North Atlantic Subpolar Gyre

[29] The North Atlantic subpolar gyre (NASPG) is defined as the area stretching from 44°N to 70°N and 10°W to 60°W. Regional analysis is limited to the 6-year period October 1997 to September 2003, because of a shorter temporal coverage of MICOM2 MLD. March averages are used to illustrate typical winter conditions instead of January owing to the lack of ocean color information in January poleward of ~50°N. Summer conditions are represented by July averages, as for the global analysis.

[30] TOPS only considers the upper 400 m of water column, and hence produces the shallowest winter mixed layer (Table 2). In contrast, HYCOM MLD is by far the deepest. Despite the pronounced differences in average March MLD among the models, the related NPP values are remarkably similar. This is notable in most of the statistics for average March NPP shown in Table 2. In average July, on the other hand, the mean and median of HYCOM MLD are ~10 m smaller than the equivalent statistics of TOPS, MICOM1 and MICOM2 MLD data sets (Table 2). Being the shallowest, HYCOM mixed layer results in the highest NPP, with the mean and median

~150 to ~200 mg C m^{-2} d^{-1} above average July NPP based on MLD input from the other three models.

[31] The seasonal character of the relationship between MLD and NPP in NASPG is clearly evident on maps of average differences between pairs of modeled MLD fields and the resulting differences in NPP fields (Figures 3a–3l). The key results for comparison between TOPS and MICOM1 in NASPG are same as outlined in section 3.1 for middle to high latitudes. Findings for the remaining pairs of models also generally agree with the results reported in the global analysis (remarkable ΔMLD during winter accompanied by insignificant ΔNPP; small ΔMLD in summer cooccurring with pronounced ΔNPP). Here, we focus on the summer findings.

[32] In average July, the two versions of MICOM show close agreement in their MLD values so that |ΔMLD| is mostly less than 10 m (Figure 3g). The largest difference occurs in the Iceland Sea, where MICOM1 estimates ~70 m deeper mixed layer. Despite the generally high level of similarity in MLD estimates, considerable differences in NPP values are present over a large part of the gyre area (Figure 3h). Even a difference in MLD of less than one meter can lead to more than 100 mg C m^{-2} d^{-1} difference in NPP. Thus, |ΔNPP| is largest in the Iceland Sea (up to ~1000 mg C m^{-2} d^{-1}). However, looking at the whole gyre region, the comparison of the two MICOM-based NPP data sets does not reveal as strong differences as those found when MICOM1 is compared with TOPS (Figure 3d).

[33] While the comparisons between TOPS and MICOM1, as well as MICOM1 and MICOM2, show both regions of negative and positive ΔMLD, average July mixed layer from HYCOM is almost invariably shallower than that from MICOM2 (Figure 3k). The bulk of ΔMLD values range up to ~20 m. In contrast, the majority of ΔNPP values are negative, spreading mostly between about −10 and −600 mg C m^{-2} d^{-1}, with only a small number of values over −1000 mg C m^{-2} d^{-1} (Figure 3l). Positive ΔNPP is very rare and close to zero.
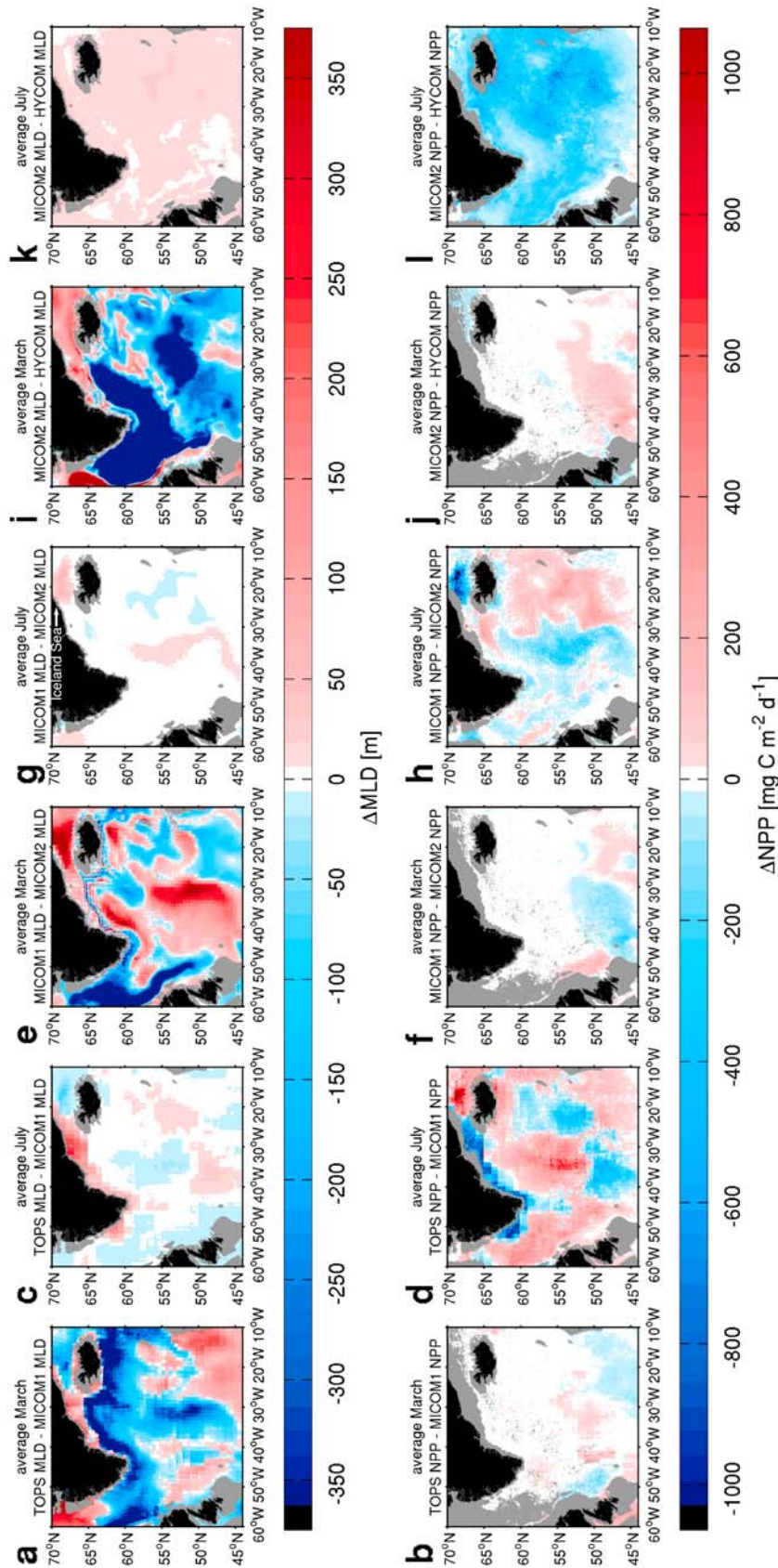
Figure 3. Differences in average March and July MLD (ΔMLD [m]) and the corresponding differences in NPP (ΔNPP [mg C m^{-2} d^{-1}]) in NASPG, for the period 1998–2003, between (a–d) TOPS and MICOM1, (e–h) MICOM1 and MICOM2, and (i–l) MICOM2 and HYCOM. Grey color denotes shelf (<200 m) and locations without available MLD or ocean color data.
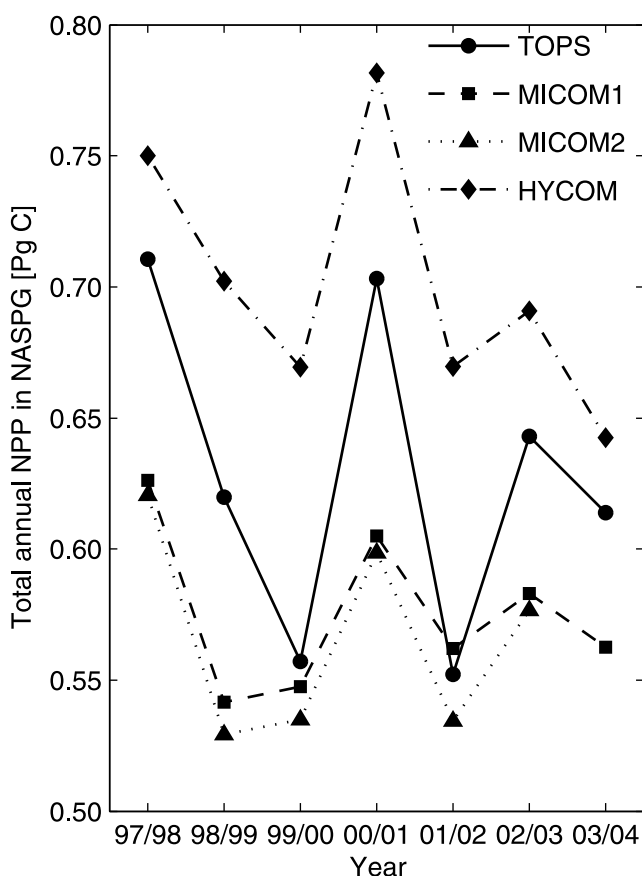
Figure 4. Areally integrated annual NPP [Pg C] in the North Atlantic subpolar gyre, calculated by the DWI CbPM, using MLD input from TOPS, MICOM1, MICOM2, and HYCOM, respectively. Note that the y axis does not start from zero. Each year is defined as a 12-month period from October to September, starting with October 1997. There are no data from MICOM2 for the last year in the time series. Shelf regions (<200 m) are not taken into account. Cloud correction has not been performed. Thus, these NPP estimates are somewhat lower than they would be if cloudiness were "removed."

[34] The substantial differences in NPP values, characteristic of summer in NASPG, translate into considerable differences in regionally integrated annual NPP (Figure 4). The consistently lowest annual NPP arises from MICOM2 MLD. MICOM1 MLD yields only slightly higher annual NPP. In comparison, total annual NPP values based on TOPS MLD are substantially larger ($\sim$10–17%), except in years 1999/2000 and 2001/2002. The HYCOM MLD results in the highest annual NPP values for the whole period, between $\sim$5 and $\sim$20% above the corresponding annual NPP estimates based on TOPS MLD. We have found that peaks in all annual NPP estimates during the years 1997/1998 and 2000/2001 seem to be mostly due to larger average values of $b_{bp}(443)$ in those years. The contribution of other input variables to the observed annual NPP peaks, particularly those that have a highly nonlinear relationship with the model-derived NPP (i.e., $K_d(490)$ and MLD), is less clear.

3.3. Eastern North Atlantic Subtropical Gyre

[35] As in the case of NASPG, only the 6-year period between October 1997 and September 2003 is considered for the eastern part of the North Atlantic subtropical gyre (NASTG-E), defined as the area between 20°W–40°W and 25°N–40°N. Differences in monthly MLD averages between June and October are found to be very small, while the accompanying NPP differences are almost nonexistent. Average ΔMLD and ΔNPP in winter and early spring months are, in comparison, much stronger. Thus, we focus on results for winter represented by average February, which is the month when the NPP estimates generally reach annual minimum and disagree the most.

[36] TOPS produces the shallowest mixed layer estimates (centered at $\sim$105 m), which result in overall the highest average February NPP values (clustered around $\sim$390 mg C m^{-2} d^{-1}; Table 3). MLD data from the two versions of MICOM are somewhat larger, thus resulting in lower NPP. Finally, HYCOM MLD values are largest (with the median $\sim$90 m greater than that of TOPS MLD) and translate into the lowest NPP values, with the median nearly 280 mg C m^{-2} d^{-1} lower than that of TOPS-based NPP.

[37] Figures 5a–5f illustrate the average February relationship between ΔMLD and ΔNPP geographically. Average February ΔMLD values between TOPS and MICOM1 in NASTG-E are predominantly negative, but do not go beyond about −60 m (Figure 5a). A narrow band with positive ΔMLD reaching up to $\sim$40 m is encountered in the northern part of the region. Figure 5b reveals a dominant pattern of positive ΔNPP values, majority of which extend up to $\sim$270 mg C m^{-2} d^{-1}, and a minor patch of negative ΔNPP ranging down to $\sim$−65 mg C m^{-2} d^{-1}.

[38] In comparison, ΔMLD and ΔNPP values between MICOM1 and MICOM2 display roughly opposite structures (Figures 5c–5d). The majority of ΔMLD values are located between about −50 and +50 m. Only a small portion of ΔNPP reaches beyond about −175 or +95 mg C m^{-2} d^{-1}.

[39] Average February ΔMLD is most pronounced between MICOM2 and HYCOM data (Figure 5e), from about −170 to +35 m and negative values predominate. The corresponding ΔNPP values lie mainly between about −65 and +340 mg C m^{-2} d^{-1} and are mostly positive (Figure 5f). However, in the northwestern corner of NASTG-E both ΔMLD and ΔNPP are negative. Examination of the data from each February between 1998 and 2003 reveals that negative ΔMLD predominates in this part of the gyre. However, it often fails to exert much effect on NPP. On the other hand, positive ΔMLD is regularly associated with fairly pronounced negative ΔNPP. Consequently, the process of averaging obscures the true nature of the relationship between ΔMLD and ΔNPP here.

[40] Table 3 shows that all models produce considerably shallower mixed layer in summer than in winter. Summer MLD exceeds 50 m in few cases. HYCOM MLD is the shallowest. TOPS MLD is the second shallowest (both in terms of mean and median). Data sets from the two versions of MICOM are not very much different (see also Table 4). NPP estimates differ at most by a few milligrams of carbon per square meter per day (Table 4).

Table 3. Descriptive Statistics of Respective MLD Values From TOPS, MICOM1, MICOM2, and HYCOM, and Their Associated NPP Values in the Eastern Part of the North Atlantic Subtropical Gyre in Average February and July of the Period 1998–2003[a]

	MLD				NPP			
	TOPS	MICOM1	MICOM2	HYCOM	TOPS	MICOM1	MICOM2	HYCOM
				Average February				
Mean	109.0	137.4	130.3	191.6	359.6	238.4	276.3	142.5
Median	105.4	137.5	125.5	196.0	392.4	210.2	285.7	115.0
Minimum	81.0	104.8	99.7	98.7	14.0	24.7	8.4	0.7
Maximum	176.2	201.6	211.6	294.3	4307.5	2066.8	3824.5	925.2
2nd percentile	87.7	108.9	107.4	118.2	55.3	75.9	36.9	3.9
98th percentile	155.6	171.4	189.9	263.8	575.6	481.6	522.0	394.5
				Average July				
Mean	22.4	26.8	25.9	16.6	570.6	570.6	570.6	570.9
Median	18.7	25.9	24.7	14.5	569.2	569.4	569.5	569.7
Minimum	12.7	21.1	20.5	7.2	366.7	367.2	367.3	367.4
Maximum	51.2	41.0	45.0	38.1	1512.4	1504.0	1504.0	1510.9
2nd percentile	14.3	21.5	21.0	8.4	412.9	413.0	413.0	413.1
98th percentile	45.4	38.4	40.2	32.3	730.8	730.5	730.5	731.1

[a]Locations shallower than 200 m are not taken into account.

[41] The findings in NASTG-E are largely opposed to those reported for NASPG. During winter, which is the season of the deepest mixed layer and strongest ΔMLD, ΔNPP is most pronounced. During summer, the mixed layer is at its shallowest and NPP at its highest. However, ΔMLD and particularly ΔNPP are insignificant.

[42] Regionally integrated annual NPP estimates in NASTG-E are presented in Figure 6. TOPS-based NPP
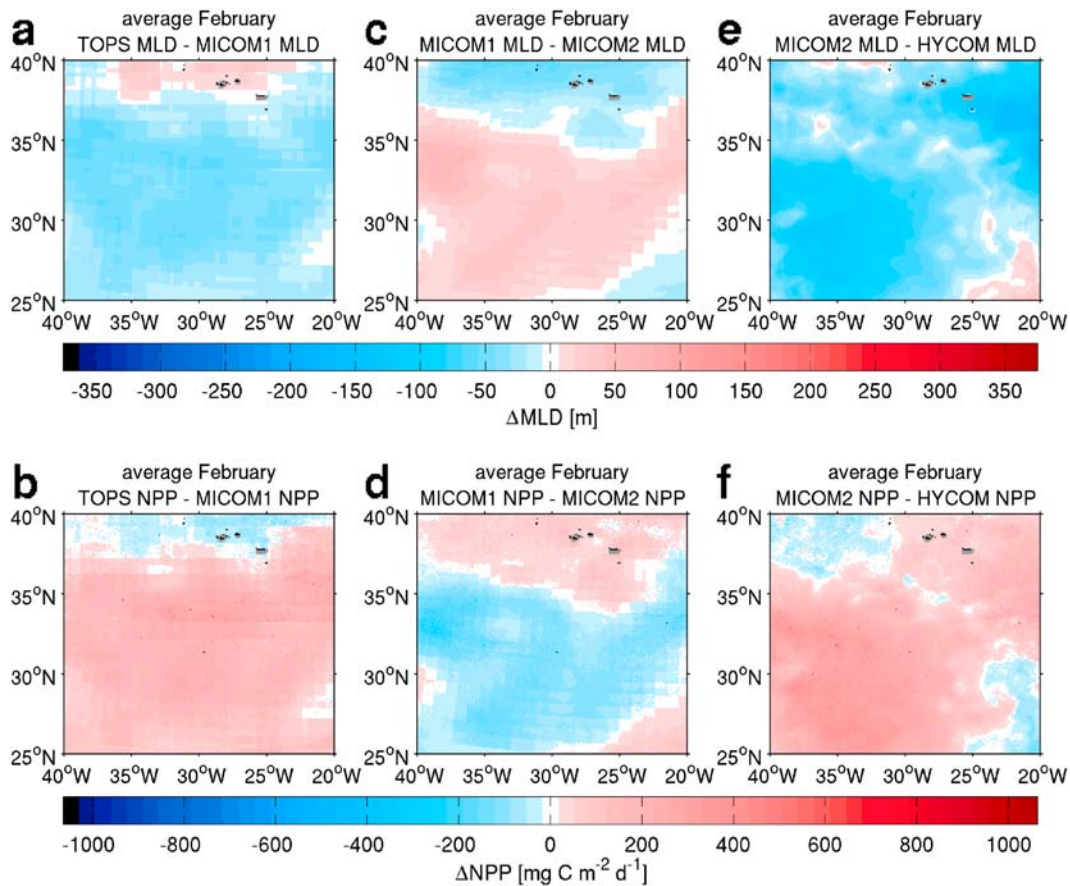
Figure 5. Differences in average February MLD (ΔMLD [m]) and the corresponding differences in NPP (ΔNPP [mg C m^{-2} d^{-1}]) in NASTG-E for the period 1998–2003. (a) ΔMLD between TOPS and MICOM1 and (b) the associated ΔNPP; (c) ΔMLD between MICOM1 and MICOM2 and (d) the related ΔNPP; (e) ΔMLD between MICOM2 and HYCOM and (f) the corresponding ΔNPP. Grey color represents locations shallower than 200 m and grid cells where MLD or ocean color data are unavailable.

Table 4. Descriptive Statistics of Respective Differences in Mixed Layer Depth Fields Produced by TOPS, MICOM1, MICOM2, and HYCOM, and the Associated Differences in Net Primary Productivity Fields in the Eastern Part of the North Atlantic Subtropical Gyre in Average July of the Period 1998–2003[a]

|	ΔMLD			ΔNPP		
	TOPS – MICOM1	MICOM1 – MICOM2	MICOM2 – HYCOM	TOPS – MICOM1	MICOM1 – MICOM2	MICOM2 – HYCOM
Average July						
Mean	−4.4	0.8	9.3	0.0	0.0	−0.3
Median	−6.1	0.9	10.0	0.1	0.0	−0.2
Minimum	−11.9	−4.8	−3.4	−7.7	−2.3	−14.0
Maximum	17.1	4.1	15.4	8.4	6.1	4.0
2nd percentile	−10.3	−2.1	0.8	−1.9	−0.2	−1.4
98th percentile	10.1	2.7	13.6	0.8	0.5	0.0

[a]Locations shallower than 200 m are not taken into account.

estimates are highest during the whole period of the study. They exceed the estimates based on MLD from the two MICOM versions by 2–7%. TOPS-based values are 15–23% above the consistently lowest HYCOM-based values.

4. Discussion

[43] Accurate assessments of ocean NPP depend, inter alia, on representation of phytoplankton exposure to light. Growth irradiance (I_g) is strongly influenced by variations in vertical mixing [e.g., *MacIntyre et al.*, 2000, 2002]. Our study focused on the part of uncertainty in I_g (and thus NPP) arising from uncertainty in MLD, by applying a selection of modeled MLD estimates to the DWI CbPM. The global analysis of modeled MLD fields and associated NPP fields reveals a generally inverse relationship. It is specified in equations (1) and (3) that shallower mixed layer results in higher average irradiances, leading to higher growth rates and hence increased NPP. In contrast, large MLD limits light availability and, in turn, NPP. It is important to note that mixed layer depth affects NPP both by influencing the availability of light and nutrients for photosynthesis. However, there is a trade-off between the two effects, as light availability drops, whereas nutrient availability increases with deepening mixing [*Mann and Lazier*, 1996]. In the model considered here, MLD is used explicitly to determine growth irradiance only. On the other hand, the model takes into account the effect of MLD on nutrient levels indirectly via Chl:C ratio. Here, we investigated the relationship between MLD and NPP that is explicit in the DWI CbPM. Our findings show the influence of MLD uncertainties on NPP assessments is highly variable, ranging from no effect to a strong inverse relationship. Our analysis suggests that this can be explained by the following factors: (1) The dependence of I_g on MLD (equation (3)) is not linear. (2) The impact of MLD on I_g is conditioned by $K_d(490)$ and I_0. These conclusions are robust to the influence of cloudiness on NPP averages, on which this analysis is based.

[44] The relationship between ΔMLD and ΔNPP is found to have a seasonal character. In general, greater absolute values of ΔMLD (|ΔMLD|) are present during winter. Middle and high latitudes in the winter hemisphere have more pronounced ΔMLD than lower latitudes. In contrast, winter |ΔNPP| at middle to high latitudes is minor, while summer |ΔNPP| is considerably larger. In subtropical ocean
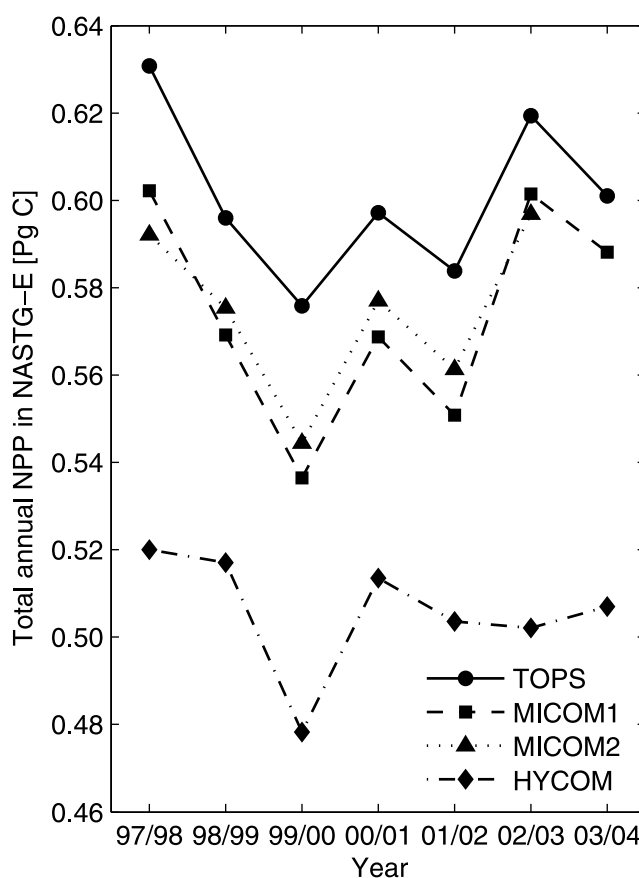
Figure 6. Areally integrated annual NPP [Pg C] in the eastern part of the North Atlantic subtropical gyre, calculated by the DWI CbPM using MLD input from TOPS, MICOM1, MICOM2, and HYCOM, respectively. Note that the *y* axis does not start from zero. Each year is defined as a 12-month period from October to September, starting with October 1997. Data from MICOM2 are unavailable for the last 12 months of the time period. Although NPP fields have not been corrected for cloudiness, cloud presence in this region is rather small, especially in summer months. Therefore, these estimates are probably not very much lower than they would be if cloud correction were performed.

gyres, on the other hand, a different seasonal regime is encountered. In summer, when $|\Delta MLD|$ is minimal, there is virtually no difference in NPP. In winter, ΔMLD is much more prominent and ΔNPP is more distinct. A rare region that does not display seasonal differences is the equatorial Pacific, where persistently small or moderate $|\Delta MLD|$ is coupled with large $|\Delta NPP|$.

[45] Two previous studies have addressed the influence of MLD perturbations on several NPP models [Carr et al., 2006; Friedrichs et al., 2009]. Carr et al. [2006] studied the impact of wide-range variations in MLD on six NPP models at 11 points representative of conditions in different ocean basins. Two models were relatively insensitive to ΔMLD, while the rest showed considerable sensitivity, but usually less than a factor of two. They found the sensitivity was largest during respective summer at locations in the temperate North Atlantic (51.3°N, 21.8°W), subtropical North Pacific (33.8°N, 153.9°E) and subtropical Indian Ocean (36.6°S, 83.7°E), where initial MLD was 10–15 m. Our results agree with those of Carr et al. [2006] at the mid-latitude North Atlantic location, but we found no sensitivity in NPP at the subtropical latitudes.

[46] A recent study by Friedrichs et al. [2009] analyzed the effect of uncertainties in MLD on seven NPP models, including the DWI CbPM, in the tropical Pacific. The skill of most NPP models was seriously affected by MLD perturbations of ±20 m. The impact on the DWI CbPM was largest. Friedrichs et al. [2009] found that eliminating MLD uncertainties would greatly improve the DWI CbPM performance in the tropical Pacific, as it may lower the related total root mean square difference by up to 40%. This is consistent with our results in the same region. It should be noted that the CbPM has recently been significantly expanded to include spectral- and depth-dependent variations in light properties, phytoplankton biomass and growth rate [Westberry et al., 2008]. This depth- and wavelength-resolved (DWR) CbPM was also subjected to MLD perturbations by Friedrichs et al. [2009]. Unlike its predecessor, it showed little sensitivity. We compared the sensitivity of NPP estimates from both versions of the CbPM at three respective locations in NASPG (48.81°N, 43.80°W), NASTG-E (33.06°N, 37.05°W) and the equatorial Pacific (0.88°S, 150.99°W). Each location corresponds to a 9-km SeaWiFS bin and is representative of seasonal variability in input values and model response in a given region. Values of input variables were taken from March and July 2000 in NASPG, while January and July 2000 were used elsewhere. The model runs were performed as described in section 2.4, with the addition of nitracline depth as input for the DWR CbPM (computed by the method of Westberry et al. [2008], but based on more recent climatological nutrient fields [Garcia et al., 2006]). Figures S1–S3 of the auxiliary material show that while the two CbPM versions give rather different results, their sensitivity to uncertainties in MLD is generally comparable.[1] A somewhat smaller sensitivity of the DWR CbPM is observed in July 2000 in NASPG and the equatorial Pacific. The tendency of the DWI CbPM to give higher NPP is mainly due to overestimated Z_{eu} values in this model version [Westberry et al., 2008]. When Z_{eu} values estimated by the method of Westberry et al. [2008] are used instead to get the total water column NPP from the surface NPP estimates of the DWI CbPM, the results are much closer to those of the DWR CbPM (Figures S1–S3). The findings of our brief analysis in the equatorial Pacific do not seem to comply with those of Friedrichs et al. [2009], perhaps because they used smaller MLD perturbations. Thus, a separate study is required to analyze the sensitivity of the DWR CbPM to MLD in more detail and so fully identify the corresponding differences and similarities between the two model versions.

[47] Mechanisms responsible for the observed difference in seasonal regimes between higher and lower latitudes are revealed by a closer inspection of the NASPG and NASTG-E results. In NASPG, winter ΔMLD is very distinct and often reaches several hundred meters. However, this yields minor difference in NPP due to generally unfavorable irradiance conditions. Photoperiod during winter is short, while surface photosynthetically available radiation (I_0) is low. These circumstances, combined with large MLD, suppress productivity. In order to illustrate reasons for this finding, we rearranged equation (3):

$$MLD = \frac{2}{K_d(490)} \times \left[\ln(I_0) - \ln(I_g) \right]. \qquad (4)$$

[48] The fourth term in equation (1), $(1 - e^{-3I_g})$, implies a threshold value of I_g below which productivity is limited by light. We approximated this threshold to 2 mol photons m^{-2} h^{-1}. Applying it to equation (4) for a range of I_0 and $K_d(490)$ gives a set of MLD values on the verge of light limitation (see Figure 7a). If modeled MLD for a given pair of coincident I_0 and $K_d(490)$ values is smaller than the associated threshold MLD value in Figure 7a, the presence of light saturation is indicated. Regardless of how much MLD estimates differ among the models, if they are all smaller than the threshold MLD, NPP values derived from them will be equal (i.e., highest possible for particular nutrient and temperature levels). When modeled MLD exceeds the threshold MLD value, light limitation is at work. The larger the modeled MLD gets, the stronger the light limitation becomes. However, this is only true until MLD renders I_g so small that we can regard it as being effectively 0 mol photons m^{-2} h^{-1}. Figure 7b shows MLD values at which this critical point is reached, for an array of I_0 and $K_d(490)$. At and beyond this point, light limitation can be considered complete. Thus, when MLD estimates from different models enter the realm of full light limitation, their associated NPP estimates must be the same, namely 0 mg C m^{-2} d^{-1}.

[49] In NASPG in March, I_0 is usually so low that full light saturation cannot be achieved (Figure 7a). Full light limitation may be reached at depths between ~40 and ~200 m (Figure 7b), depending on the combination of typical I_0 and $K_d(490)$ values. The vast majority of MLD estimates are $\geq$~200 m (see Figure 7c), making the related NPP values negligible. Therefore, the largest part of NASPG is characterized by zero ΔNPP during winter.
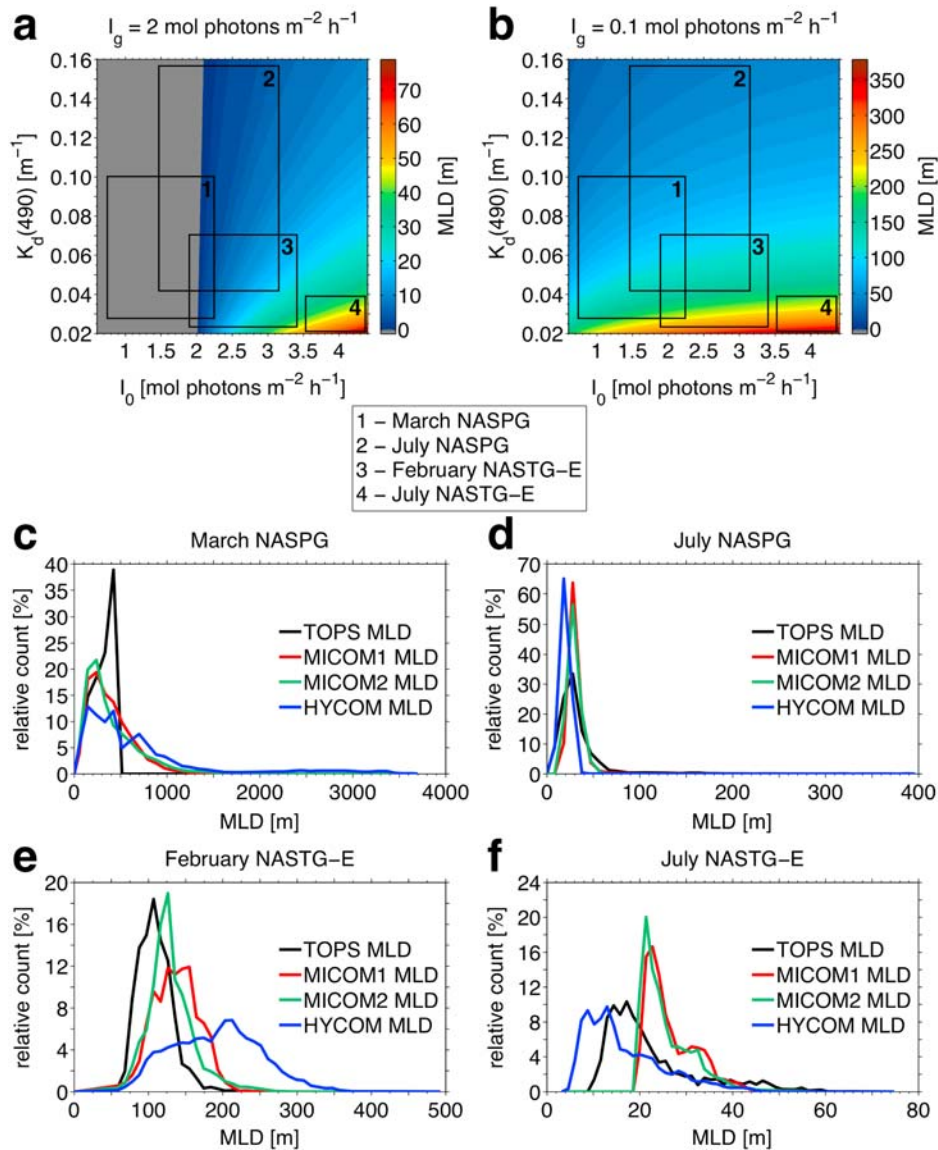
Figure 7. (a) Two-dimensional filled contour graph showing critical MLD as a function of I_0 [mol photons m^{-2} h^{-1}] and $K_d(490)$ [m^{-1}] for $I_g = 2$ mol photons m^{-2} h^{-1} (see equation (4)). (b) Same as Figure 7a, but for $I_g = 0.1$ mol photons m^{-2} h^{-1}. The rectangles superimposed on the graphs show typical ranges of I_0 and $K_d(490)$ values for (1) March and (2) July in NASPG, and (3) February and (4) July in NASTG-E, respectively. These ranges are defined as 95% quantile intervals between 2.5 and 97.5% quantiles of the observed I_0 and $K_d(490)$ values for each respective month between 1998 and 2003. Note that the color scales in Figures 7a and 7b have different extent. Grey in Figure 7a denotes circumstances in which no light saturation is possible. Figures 7c–7f show relative count (i.e., relative frequency distributions) of MLD values modeled by TOPS, MICOM1, MICOM2, and HYCOM, respectively, in representative months from 1998 to 2003: (c) March in NASPG; (d) July in NASPG; (e) February in NASTG-E; (f) July in NASTG-E. Relative counts were calculated as follows: In a particular region, MLD values estimated by a given ocean model in a certain month from 1998 to 2003 were collected together. Values from shelf areas were omitted. The range of MLD values was divided into equally spaced class intervals. Number of values in each class interval was determined and then divided by the total number of values.

Toward summertime, MLD becomes shallower owing to the combined effect of rising sea surface temperatures, weaker winds and increased freshwater (meltwater) fluxes. All ocean models estimate this shoaling and ΔMLD becomes less prominent. NPP and $|\Delta$NPP$|$, however, soar to summer maxima. Figures 7a–7b illustrate how the coexisting I_0 and $K_d(490)$ values characteristic of July in NASPG influence the threshold MLD values. Figure 7d

shows that MLD from the two MICOM models is too large for full light saturation to be achieved. On the other hand, TOPS and particularly HYCOM MLD can theoretically often result in I_g equal to or larger than the saturation threshold. Nevertheless, we have found that matching I_0 and $K_d(490)$ are seldom favorable enough and only ~4% of MLD estimates from the latter two models give light saturated photosynthesis. Full light limitation is similarly rare. Depending on model, 90 to 99% of MLD estimates result in partial light limitation. Differences between these estimates, although small, have potential to trigger rather large differences in I_g because they are often coupled with rapid decay of light in the water column (see the range of $K_d(490)$ in Figures 7a–7b). This is in turn translated into considerable ΔNPP.

[50] In comparison, the largest winter $|\Delta MLD|$ values in NASTG-E are accompanied by the largest $|\Delta NPP|$. Figures 7a–7b reveal the interactions among MLD, I_0 and $K_d(490)$ underlying this finding. No model estimates a sufficiently shallow mixed layer for full light saturation to be accomplished (Figure 7e). The range of winter MLD values from TOPS, MICOM1 and MICOM2 is such that, combined with the prevalent illumination conditions, partial light limitation occurs in 70 to 80% of cases. HYCOM MLD is considerably deeper and leads to full light limitation in more than 50% of instances. In summer, ΔMLD in NASTG-E is small and ΔNPP practically zero (Table 4), which differs from the relationship in NASPG. This is explained by the combination of shallow summer mixed layer (Figure 7f) with high I_0 and low $K_d(490)$ values, which in almost all cases leads to I_g exceeding the saturation threshold value (see Figure 7a), thus causing no difference in NPP.

[51] To recapitulate, seasonal development of $|\Delta NPP|$ in NASPG runs in parallel with the seasonal cycle of NPP, rising from a winter minimum to a summer maximum. In this regime, it is the summer MLD values that bear most importance for NPP estimates, whereas winter ΔMLD makes little difference. On the other hand, the seasonal cycle of ΔNPP in NASTG-E is in antiphase with the seasonal changes in NPP itself: most distinct ΔNPP occurs in low productivity period, while summertime ΔNPP is virtually zero. In this case, variability in MLD between June and October has practically no discernable influence on NPP, while winter ΔMLD has the largest impact.

[52] $K_d(490)$ can be used to indicate how sensitive NPP is to changes in MLD. For the same I_0, increase in $K_d(490)$ causes the depth of transition from saturating to limiting I_g to be shallower (Figure 7a). The same is valid for the depth at which total light limitation arises (Figure 7b). Also, the difference between the two critical MLD values for a given I_0 becomes smaller as $K_d(490)$ increases. For example, for $I_0 = 3$ mol photons m^{-2} h^{-1} and $K_d(490) = 0.02$ m^{-1}, the progression from full light saturation (MLD = 40.5 m) to full light limitation (MLD = 340 m) occurs over a range of ~300 m (compare Figures 7a and 7b). However, the critical depth difference becomes only 37.5 m (i.e., 42.5 − 5 m) for the same I_0 when $K_d(490)$ is 0.16 m^{-1}. It follows that a unit of change in MLD between the two critical values produces a steeper gradient in I_g for larger $K_d(490)$.

[53] The highest annual productivity estimates are about 20−30% above the lowest ones in NASPG, ~15 to ~20% in NASTG-E and less than 10% in the global ocean. These results are well within the factor of 2 boundaries reported for differences in global or regional annual NPP estimates in studies that compared performance of a number of different productivity algorithms [*Campbell et al.*, 2002; *Carr et al.*, 2006; *Friedrichs et al.*, 2009]. In other words, uncertainties in global or regional NPP estimates that originate from using different input MLD in a particular NPP model are much more constrained than those stemming from using different productivity models.

5. Future Directions

[54] The newly developed, more complex version of the CbPM [*Westberry et al.*, 2008] is capable of resolving vertical profiles of optical and biological properties below the mixed layer. While *Friedrichs et al.* [2009] reported its sensitivity to MLD perturbations in the tropical Pacific was much lower compared to the simpler CbPM version, we found no similar disparity between the two versions. However, as we only performed a brief comparison, further more detailed and extensive analysis is needed to fully quantify and understand the response of the more recent version of the CbPM to MLD uncertainties in various ecological regimes across the ocean.

[55] Turbulent mixing has a strong influence on vertical motion of phytoplankton cells and light intensity they experience [*MacIntyre et al.*, 2000]. However, the aim of phytoplankton productivity models to improve NPP estimates by explicitly taking the effects of vertical mixing into account is currently limited by the availability of alternatives to MLD. The concept of the mixed layer is based on the homogeneity of vertical density profile, while identification of the mixing layer depends on the dissipation rate of turbulent kinetic energy [*Dewey and Moum*, 1990]. Hence, vertical mixing of phytoplankton may be considerably shallower than MLD [e.g., *Townsend et al.*, 1994]. In other words, a deep mixed layer does not inevitably imply a severe light limitation of photosynthesis [*Backhaus et al.*, 2003; *D'Asaro*, 2008; *Huisman et al.*, 1999; *Townsend et al.*, 1994; *Yamazaki and Kamykowski*, 1991]. While the depth of active turbulent mixing would be a more adequate indicator of average growth irradiance than MLD, it is not yet a routine product of ocean modeling. Global and regional ocean models typically have too coarse horizontal resolutions to adequately resolve small-scale turbulent and convective processes that are responsible for vertical mixing [*Marshall and Schott*, 1999]. The horizontally averaged effects of these "subgrid" processes thus have to be parameterized. A number of vertical mixing parameterizations have been developed [*Burchard and Petersen*, 1999], but they are not equally skilful in realistic representation of mixing for various applications [*Burchard*, 2002]. Future activities toward advancing representation of phytoplankton light exposure should focus on selecting a theoretically sound and computationally economic turbulent mixing scheme that is best suited for this purpose.

[56] Moreover, further studies are needed to verify the existence and extensiveness of the mechanism of "phytoconvection" [*Backhaus et al.*, 2003; *D'Asaro*, 2008], which is claimed to promote phytoplankton productivity in a deep convective mixed layer during winter at high latitudes. If the importance of phytoconvection is shown to be fundamental, the widespread view that virtually no net productivity is possible at subpolar latitudes during winter will have to be reexamined.

[57] Finally, it is important to recognize that input variables other than MLD contribute to the uncertainty in model NPP estimates. For example, *Friedrichs et al.* [2009] evaluated response of a number of NPP models, including the two CbPM versions, to perturbations in Chl and I_0 in the tropical Pacific. More studies of that kind are necessary to direct future research aimed at reducing uncertainties in ocean NPP modeling.

References

Backhaus, J. O., E. N. Hegseth, H. Wehde, X. Irigoien, K. Hatten, and K. Logemann (2003), Convection and primary production in winter, *Mar. Ecol. Prog. Ser.*, 251, 1–14, doi:10.3354/meps251001.

Banse, K. (1991), Rates of phytoplankton cell division in the field and in iron enrichment experiments, *Limnol. Oceanogr.*, 36(8), 1886–1898.

Behrenfeld, M. J., and P. G. Falkowski (1997a), A consumer's guide to phytoplankton primary productivity models, *Limnol. Oceanogr.*, 42(7), 1479–1491.

Behrenfeld, M. J., and P. G. Falkowski (1997b), Photosynthetic rates derived from satellite-based chlorophyll concentration, *Limnol. Oceanogr.*, 42(1), 1–20.

Behrenfeld, M. J., W. E. Esaias, and K. R. Turpie (2002a), Assessment of primary production at the global scale, in *Phytoplankton Productivity: Carbon Assimilation in Marine and Freshwater Ecosystems*, edited by P. J. le B. Williams et al., pp. 156–186, Blackwell Sci., Oxford, U. K.

Behrenfeld, M. J., E. Maranon, D. A. Siegel, and S. B. Hooker (2002b), Photoacclimation and nutrient-based model of light-saturated photosynthesis for quantifying oceanic primary production, *Mar. Ecol. Prog. Ser.*, 228, 103–117, doi:10.3354/meps228103.

Behrenfeld, M., E. Boss, D. Siegel, and D. Shea (2005), Carbon-based ocean productivity and phytoplankton physiology from space, *Global Biogeochem. Cycles*, 19(1), GB1006, doi:10.1029/2004GB002299.

Bleck, R. (2002), An oceanic general circulation model framed in hybrid isopycnic-Cartesian coordinates, *Ocean Modell.*, 4(1), 55–88, doi:10.1016/S1463-5003(01)00012-9.

Bleck, R., and L. T. Smith (1990), A wind-driven isopycnic coordinate model of the North and Equatorial Atlantic Ocean: 1. Model development and supporting experiments, *J. Geophys. Res.*, 95(C3), 3273–3285, doi:10.1029/JC095iC03p03273.

Bleck, R., C. Rooth, D. Hu, and L. T. Smith (1992), Salinity-driven thermocline transients in a wind- and thermohaline-forced isopycnic coordinate model of the North Atlantic, *J. Phys. Oceanogr.*, 22(12), 1486–1505, doi:10.1175/1520-0485(1992)022<1486:SDTTIA>2.0.CO;2.

Burchard, H. (2002), *Applied Turbulence Modelling in Marine Waters*, 229 pp., Springer, Berlin.

Burchard, H., and O. Petersen (1999), Models of turbulence in the marine environment: A comparative study of two-equation turbulence models, *J. Mar. Syst.*, 21(1–4), 29–53, doi:10.1016/S0924-7963(99)00004-4.

Campbell, J., et al. (2002), Comparison of algorithms for estimating ocean primary production from surface chlorophyll, temperature, and irradiance, *Global Biogeochem. Cycles*, 16(3), 1035, doi:10.1029/2001GB001444.

Carr, M.-E., M. A. M. Friedrichs, M. Schmeltz, M. Noguchi Aita, D. Antoine, K. R. Arrigo, I. Asanuma, O. Aumont, R. Barber, and M. Behrenfeld (2006), A comparison of global estimates of marine primary production from ocean color, *Deep Sea Res., Part II*, 53(5–7), 741–770, doi:10.1016/j.dsr2.2006.01.028.

Clancy, R. M., and P. J. Martin (1981), Synoptic forecasting of the oceanic mixed layer using the Navy's operational environmental database: Present capabilities and future applications, *Bull. Am. Meteorol. Soc.*, 62(6), 770, doi:10.1175/1520-0477(1981)062<0770:SFOTOM>2.0.CO;2.

Clancy, R. M., and K. D. Pollak (1983), A real-time synoptic ocean thermal analysis/forecast system, *Prog. Oceanogr.*, 12(4), 383–424, doi:10.1016/0079-6611(83)90001-0.

Clancy, R. M., and W. D. Sadler (1992), The Fleet Numerical Oceanography Center suite of oceanographic models and products, *Weather Forecast.*, 7(2), 307–327, doi:10.1175/1520-0434(1992)007<0307:TFNOCS>2.0.CO;2.

Cloern, J. E., and R. Dufford (2005), Phytoplankton community ecology: Principles applied in San Francisco Bay, *Mar. Ecol. Prog. Ser.*, 285, 11–28, doi:10.3354/meps285011.

D'Asaro, E. A. (2008), Convection and the seeding of the North Atlantic bloom, *J. Mar. Syst.*, 69(3–4), 233–237, doi:10.1016/j.jmarsys.2005.08.005.

Dewey, R. K., and J. N. Moum (1990), Enhancement of fronts by vertical mixing, *J. Geophys. Res.*, 95(C6), 9433–9445, doi:10.1029/JC095iC06p09433.

Duffy, J. E., and J. J. Stachowicz (2006), Why biodiversity is important to oceanography: Potential roles of genetic, species, and trophic diversity in pelagic ecosystem processes, *Mar. Ecol. Prog. Ser.*, 311, 179–189, doi:10.3354/meps311179.

Falkowski, P. G., R. T. Barber, and V. Smetacek (1998), Biogeochemical controls and feedbacks on ocean primary production, *Science*, 281(5374), 200–206, doi:10.1126/science.281.5374.200.

Falkowski, P., et al. (2000), The global carbon cycle: A test of our knowledge of Earth as a system, *Science*, 290(5490), 291–296, doi:10.1126/science.290.5490.291.

Field, C. B., M. J. Behrenfeld, J. T. Randerson, and P. Falkowski (1998), Primary production of the biosphere: Integrating terrestrial and oceanic components, *Science*, 281(5374), 237–240, doi:10.1126/science.281.5374.237.

Friedrichs, M. A. M., et al. (2009), Assessing the uncertainties of model estimates of primary productivity in the tropical Pacific Ocean, *J. Mar. Syst.*, 76(1–2), 113–133, doi:10.1016/j.jmarsys.2008.05.010.

Frouin, R., and S. F. Iacobellis (2002), Influence of phytoplankton on the global radiation budget, *J. Geophys. Res.*, 107(D19), 4377, doi:10.1029/2001JD000562.

Gabric, A. J., R. Simo, R. A. Cropp, A. C. Hirst, and J. Dachs (2004), Modeling estimates of the global emission of dimethylsulfide under enhanced greenhouse conditions, *Global Biogeochem. Cycles*, 18(2), GB2014, doi:10.1029/2003GB002183.

Garcia, H. E., et al. (2006), *World Ocean Atlas 2005*, vol. 4, *Nutrients (phosphate, nitrate, silicate)*, *NOAA Atlas NESDIS*, vol. 64, edited by S. Levitus, 396 pp., NOAA, Silver Spring, Md.

Garver, S. A., and D. A. Siegel (1997), Inherent optical property inversion of ocean color spectra and its biogeochemical interpretation: 1. Time series from the Sargasso Sea, *J. Geophys. Res.*, 102(C8), 18,607–18,625, doi:10.1029/96JC03243.

Gaspar, P., Y. Grégoris, and J.-M. Lefevre (1990), A simple eddy kinetic energy model for simulations of the oceanic vertical mixing: Tests at station papa and long-term upper ocean study site, *J. Geophys. Res.*, 95(C9), 16,179–16,193, doi:10.1029/JC095iC09p16179.

Geider, R. J., and H. L. MacIntyre (2002), Physiology and biochemistry of photosynthesis and algal carbon acquisition, in *Phytoplankton Productivity: Carbon Assimilation in Marine and Freshwater Ecosystems*, edited by P. J. le B. Williams et al. 44–77, Blackwell Sci., Oxford, U. K.

Geider, R. J., et al. (2001), Primary productivity of planet Earth: Biological determinants and physical constraints in terrestrial and aquatic habitats, *Global Change Biol.*, 7(8), 849–882, doi:10.1046/j.1365-2486.2001.00448.x.

Hátún, H., A. B. Sandø, H. Drange, B. Hansen, and H. Valdimarsson (2005), Influence of the Atlantic Subpolar Gyre on the thermohaline circulation, *Science*, 309(5742), 1841–1844, doi:10.1126/science.1114777.

Huisman, J., P. van Oostveen, and F. J. Weissing (1999), Critical depth and critical turbulence: Two different mechanisms for the development of phytoplankton blooms, *Limnol. Oceanogr.*, 44(7), 1781–1787.

International Ocean Colour Coordinating Group (IOCCG) (2000), Remote sensing of ocean colour in coastal, and other optically-complex waters, edited by S. Sathyendranath, *Rep. 3*, Dartmouth, N. S., Canada.

International Ocean Colour Coordinating Group (IOCCG) (2004), Guide to the creation and use of ocean colour, level-3, binned data products, edited by D. Antoine, *Rep. 4*, Dartmouth, N. S., Canada.

Jickells, T. D., et al. (2005), Global iron connections between desert dust, ocean biogeochemistry, and climate, *Science*, *308*(5718), 67–71, doi:10.1126/science.1105959.

Large, W. G., J. C. McWilliams, and S. C. Doney (1994), Oceanic vertical mixing: A review and a model with a nonlocal boundary layer parameterization, *Rev. Geophys.*, *32*(4), 363–403, doi:10.1029/94RG01872.

Loisel, H., E. Bosc, D. Stramski, K. Oubelkheir, and P. Y. Deschamps (2001), Seasonal variability of the backscattering coefficient in the Mediterranean Sea based on satellite SeaWiFS imagery, *Geophys. Res. Lett.*, *28*(22), 4203–4206, doi:10.1029/2001GL013863.

MacIntyre, H. L., T. M. Kana, and R. J. Geider (2000), The effect of water motion on short-term rates of photosynthesis by marine phytoplankton, *Trends Plant Sci.*, *5*(1), 12–17, doi:10.1016/S1360-1385(99)01504-6.

MacIntyre, H. L., T. M. Kana, T. Anning, and R. J. Geider (2002), Photoacclimation of photosynthesis irradiance response curves and photosynthetic pigments in microalgae and cyanobacteria, *J. Phycol.*, *38*(1), 17–38, doi:10.1046/j.1529-8817.2002.00094.x.

Mann, K. H., and J. R. N. Lazier (1996), *Dynamics of Marine Ecosystems: Biological-Physical Interactions in the Oceans*, 2nd ed., 394 pp., Blackwell Sci., Cambridge, Mass.

Maritorena, S., D. A. Siegel, and A. R. Peterson (2002), Optimization of a semianalytical ocean color model for global-scale applications, *Appl. Opt.*, *41*(15), 2705–2714, doi:10.1364/AO.41.002705.

Marshall, J., and F. Schott (1999), Open-ocean convection: Observations, theory, and models, *Rev. Geophys.*, *37*(1), 1–64, doi:10.1029/98RG02739.

Mellor, G. L., and T. Yamada (1974), A hierarchy of turbulence closure models for planetary boundary layers, *J. Atmos. Sci.*, *31*(7), 1791–1806, doi:10.1175/1520-0469(1974)031<1791:AHOTCM>2.0.CO;2.

Riebesell, U., et al. (2007), Enhanced biological carbon consumption in a high CO_2 ocean, *Nature*, *450*(7169), 545–548, doi:10.1038/nature06267.

Siegel, D. A., S. Maritorena, N. B. Nelson, D. A. Hansell, and M. Lorenzi-Kayser (2002), Global distribution and dynamics of colored dissolved and detrital organic materials, *J. Geophys. Res.*, *107*(C12), 3228, doi:10.1029/2001JC000965.

Siegel, D. A., S. Maritorena, N. B. Nelson, and M. J. Behrenfeld (2005), Independence and interdependencies among global ocean color properties: Reassessing the bio-optical assumption, *J. Geophys. Res.*, *110*, C07011, doi:10.1029/2004JC002527.

Stramski, D., R. A. Reynolds, M. Kahru, and B. G. Mitchell (1999), Estimation of particulate organic carbon in the ocean from satellite remote sensing, *Science*, *285*(5425), 239–242, doi:10.1126/science.285.5425.239.

Townsend, D. W., L. M. Cammen, P. M. Holligan, D. E. Campbell, and N. R. Pettigrew (1994), Causes and consequences of variability in the timing of spring phytoplankton blooms, *Deep Sea Res., Part I*, *41*(5–6), 747–765, doi:10.1016/0967-0637(94)90075-2.

Westberry, T., M. J. Behrenfeld, D. A. Siegel, and E. Boss (2008), Carbon-based primary productivity modeling with vertically resolved photoacclimation, *Global Biogeochem. Cycles*, *22*, GB2024, doi:10.1029/2007GB003078.

Yamazaki, H., and D. Kamykowski (1991), The vertical trajectories of motile phytoplankton in a wind-mixed water column, *Deep Sea Res., Part A*, *38*(2), 219–241.

M. J. Behrenfeld, Department of Botany and Plant Pathology, Cordley Hall 2082, Oregon State University, Corvallis, OR 97331-2902, USA. (behrenfm@science.oregonstate.edu)

J. A. Johannessen and S. Milutinović, Nansen Environmental and Remote Sensing Center, Thormøhlensgt 47, N-5006 Bergen, Norway. (johnny.johannessen@nersc.no; svetlana.milutinovic@nersc.no)

T. Johannessen, Geophysical Institute, University of Bergen, Allegt. 70, N-5020 Bergen, Norway. (Truls.Johannessen@gfi.uib.no)